Engineering 6 (2020) 680–687

Contents lists available at ScienceDirect

Engineering

journal homepage: www.elsevier.com/locate/eng

Research
Green Chemical Engineering—Article

# Nitrogen-Doped Graphene Foam as a Metal-Free Catalyst for Reduction Reactions under a High Gravity Field

Zhiyong Wang [a,b,d], Zhijian Zhao [a,d], Jesse Baucom [b], Dan Wang [a,d,*], Liming Dai [c], Jian-Feng Chen [a,d]

[a] State Key Laboratory of Organic-Inorganic Composites, Beijing University of Chemical Technology, Beijing 100029, China
[b] Department of Chemical and Biomolecular Engineering, University of California, Los Angeles, CA 90095, USA
[c] Center of Advanced Science and Engineering for Carbon (Case4Carbon), Department of Macromolecular Science and Engineering, Case School of Engineering, Case Western Reserve University, Cleveland, OH 44106, USA
[d] Research Center of the Ministry of Education for High Gravity Engineering and Technology, Beijing University of Chemical Technology, Beijing 100029, China

ARTICLE INFO

*Article history:*
Received 16 July 2019
Revised 20 September 2019
Accepted 2 December 2019
Available online 28 May 2020

*Keywords:*
High-gravity technology
Process intensification
Metal-free catalysts
Carbon nanomaterials
Catalytic reduction

ABSTRACT

Herein, we report on the effect of a high gravity field on metal-free catalytic reduction, taking the nitrobenzene (NB) reduction and methylene blue (MB) degradation as model reactions in a high-gravity rotating tube reactor packed with three-dimensional (3D) nitrogen-doped graphene foam (NGF) as a metal-free catalyst. The apparent rate constant ($k_{app}$) of the metal-free catalytic reduction of NB in the rotating tube reactor under a high gravity level of 6484*g* ($g$ = 9.81 m·s$^{-2}$) was six times greater than that in a conventional stirred reactor (STR) under gravity. Computational fluid dynamics (CFD) simulations indicated that the improvement of the catalytic efficiency was attributed to the much higher turbulent kinetic energy and faster surface renewal rate in the high-gravity tube reactor in comparison with those in a conventional STR. The structure of the 3D metal-free catalysts was stable during the reaction process under a high gravity field, as confirmed by X-ray photoelectron spectroscopy (XPS) and Raman spectra. In the other model reaction, the rate of MB degradation also increased as the high gravity level increased gradually, which aligns with the result for the NB catalytic reduction system. These results demonstrate the potential to use a high-gravity rotating packed tube reactor for the process intensification of metal-free catalytic reduction reactions.



## 1. Introduction

Carbon-based metal-free catalysts have attracted considerable attention in both academic and industrial research due to their low cost and eco-friendly properties [1–3]. By doping carbon nanomaterials with heteroatoms, the chemical activities of nanomaterials can be tuned due to electron reassignment, leading to many novel applications [4–6]. In particular, with the development of green chemistry and sustainable chemistry, metal-free carbon-based catalysts have been found to have great potential for replacing traditional metal catalysts in some typical industrial reactions [7,8]. Although laboratory research on carbon-based metal-free catalysts has achieved great successes, huge challenges remain for the industrial trials and practical applications of such catalysts [9]. Compared with those of metal matrix catalysts, the catalytic efficiencies of metal-free catalysts are lower in many cases [6]. Researchers have argued that this is due not only to the chemically active center status at the atomic level, but also to the physical structure of the catalysts, which directly affects the micromixing status in different phases in a reaction system, and thus influences the final activity of the catalyst [10]. Therefore, apart from intrinsic structural optimization of catalysts, the coupling between the catalyst and reactor is an important topic of research for industrial catalytic reactions.

Process intensification (PI) technologies based on modular chemical processing [11] and the use of external files, such as microwave [12], magnetic [13], and light [14], have recently attracted considerable attention in chemical engineering. Among them, the introduction of a high gravity field into the chemical process has been demonstrated to be an efficient approach for the intensification of micromixing and mass transfer [15]. Along with other researchers, our group has successfully applied high-gravity-assisted technologies for nanoparticles production

* Corresponding author.
*E-mail address:* wangdan@mail.buct.edu.cn (D. Wang).

https://doi.org/10.1016/j.eng.2019.12.018

[16–18], gas purification [19], and organic synthesis [20]. It is generally accepted that the high-gravity environment generated by the centrifugal force coupled with the porous packing in a reactor is beneficial for enhancing micromixing conditions and the mass-transfer effect, resulting in high-quality products [21–23]. Zhang et al. [24] measured hydrodynamic performance and mass-transfer efficiency by using porous nickel foam as the packing in a distillation column, and found that the mass-transfer efficiency of the nickel foam packing was 40% higher than that of traditional stainless-steel wire-mesh packing. Another type of porous packing, ceramic foam, was used in a cyclohexane/*n*-heptane system at atmospheric pressure under total reflux; the liquid hold-up was found to be greater than that using other classical packing materials and the performance of the mass transfer was excellent, with a height equivalent to a theoretical plate of 0.2 m due to the increasing gas and liquid superficial velocities inside the packing [25].

In this work, we report on the behaviors of the metal-free catalytic reduction of nitrobenzene (NB) under a high gravity field in a high-gravity tube reactor. Macroscopic three-dimensional (3D) nitrogen-doped graphene foam (NGF), which was prepared by the hydrothermal treatment of the aqueous dispersion of graphene oxides (GO) and urea, was used as the metal-free catalyst for both NB reduction and methylene blue (MB) degradation under a high gravity field in a rotating tube reactor. The stable performance of the 3D metal-free catalyst was measured using X-ray photoelectron and Raman spectra. These results demonstrate the potential to use high-gravity technology for the intensification of metal-free catalytic reactions.

## 2. Materials and methods

### 2.1. Preparation of 3D NGF

The GO was produced by a modified Hummers' method [26]. Typically, 50 mg GO, 2 mL of urea solution, and 25 mL of deionized water were sealed in a 50 mL Teflon-lined stainless autoclave and heated to 180 °C for 12 h to form nitrogen graphene sheets (NGS). The obtained NGS were then washed with water. After the autoclave naturally cooled to room temperature, the bulk NGF was washed with deionized water and then freeze-dried for 56 h. The sample was pre-frozen at −50 °C for 5 h. Afterward, the pressure was decreased to 1.1 Pa and the freeze-dryer was heat up to 25 °C, increasing at a rate of 1 °C·h$^{-1}$ for 20 h, 1.25 °C·h$^{-1}$ for 16 h, 1 °C·h$^{-1}$ for 10 h, and 5 °C·h$^{-1}$ for 5 h.

### 2.2. Material characterization.

Morphology and microstructure studies were performed with a Hitachi S-4700 field-emission scanning electron microscope (SEM) and a Hitachi H-9500 high-resolution transmission electron microscope (HRTEM). Fourier-transform infrared (FTIR) spectra were recorded on a Thermo Fisher spectrum Nicolet 6700 FTIR system. X-ray photoelectron spectroscopy (XPS) results were obtained using a VG Microtech ESCA 2000. Raman spectra were procured on a Raman spectrometer (Renishaw) excited with a 514 nm laser.

### 2.3. Catalytic reaction under high gravity field

For the hydrogenation of the NB catalytic reaction, a 7 mL mixture containing 2 mmol $NaBH_4$ and 0.02 mmol NB was added to a tube reactor filled with 3D structured NGF as a catalyst (6 mg). The NGF was shaped as cylinders of 10 mm in diameter and 15 mm in height. The reactor was then put into a high-speed centrifuge (Changsha Xiangyi Instrument Co., Ltd., H-1850). By adjusting the rotational speed, the metal-free catalytic reduction of NB progressed under various high gravity fields. A Shimadzu ultraviolet (UV)–visible (Vis) spectra (UV-2600) was used to monitor the absorbance of NB in the mixture and the components of the reaction products were analyzed by high-performance liquid chromatography (HPLC) (Water 2695). The absorbance spectra were measured with a W2996 photodiode array detector. For the studies of the MB degradation process, a 7 mL mixture containing 2 mmol $NaBH_4$ and 0.02 mmol MB was added in a tube reactor filled with 3D structured NGF as a catalyst (6 mg). These reactions were allowed to progress under the same aforementioned high gravity fields, and the degradation process was monitored by measuring the absorbance spectra of the MB. For comparison experiments, reactions were also conducted in the conventional stirred reactor (STR) without a high gravity field, while maintaining the other conditions of the following procedures identical to those used under the high gravity field.

### 2.4. Calculation of the high gravity level

As the mass transfer and mixing conditions are enhanced by the centrifugal force in the reactor, the mixture's status, such as shape (liquid films, liquid ligaments, droplets) distribution, mass-transfer interfacial area, and surface renewal rate, changed under various high gravity conditions. Here, a high gravity level ($G$), which reflects the high gravity field by values relative to gravitational acceleration $g$ ($g$ = 9.81 m·s$^{-2}$), is defined to describe the relation between the catalytic reaction effect and the high gravity field. It can be calculated using the following equation:

$$G = \left(\frac{2\pi N}{60}\right) \cdot R/g \tag{1}$$

where $R$ is the rotating radius of the mixture, $N$ is the rotating speed of the reactor, and $g$ is gravitational acceleration.

## 3. Results and discussion

Hydrothermal treatment of GO and urea at 180 °C is a relatively mild and economically sound method for the doping of nitrogen atoms into a graphene plane structure [27]. The high pressure produced by the solvent vapor during the synthesis process reintegrates the dispersive graphene sheets and forms cylinder-like shapes. After being cooled to room temperature and washed with a large amount of deionized water, the bulk NGF was filled with liquid in the internal hole-channel. The pores in the NGF shrunk as the liquid evaporated during direct drying in the oven, resulting in a small volume and a decreased pore diameter of the NGF. However, a freeze-dry treatment was used to remove the remnant liquid while leaving the appearance and mechanical strength of the NGF unchanged (Fig. S1). Fig. 1(a) shows the porous structure of the NGF, with a pore size ranging from several to dozens of nanometers; this distribution was further verified by Brunauer–Emmett–Teller (BET) characterization. In Fig. 1(b), the SEM image displays the typical structure and morphology of transparent NGF with wrinkled and voile-like features. Meanwhile, a combination of the SEM and transmission electron microscope (TEM) images reveals that the 3D structure of the NGF was made up of extremely thin graphene sheets (Fig. 1(c)). The HRTEM image shows the NGF crystalline structure with a lattice spacing of 0.32 nm, which was attributed to the (102) facet of graphite [7]. The corresponding element mapping of SEM images indicate that the C, N, and O elements are uniformly distributed at mesoscale (Figs. 1(e–h)).

Fig. 2(a) shows the FTIR spectrum of NGF, with characteristic peaks of C–N and C=N at 1167 and 1380 cm$^{-1}$, respectively [28], which demonstrate that the nitrogen atoms were successfully

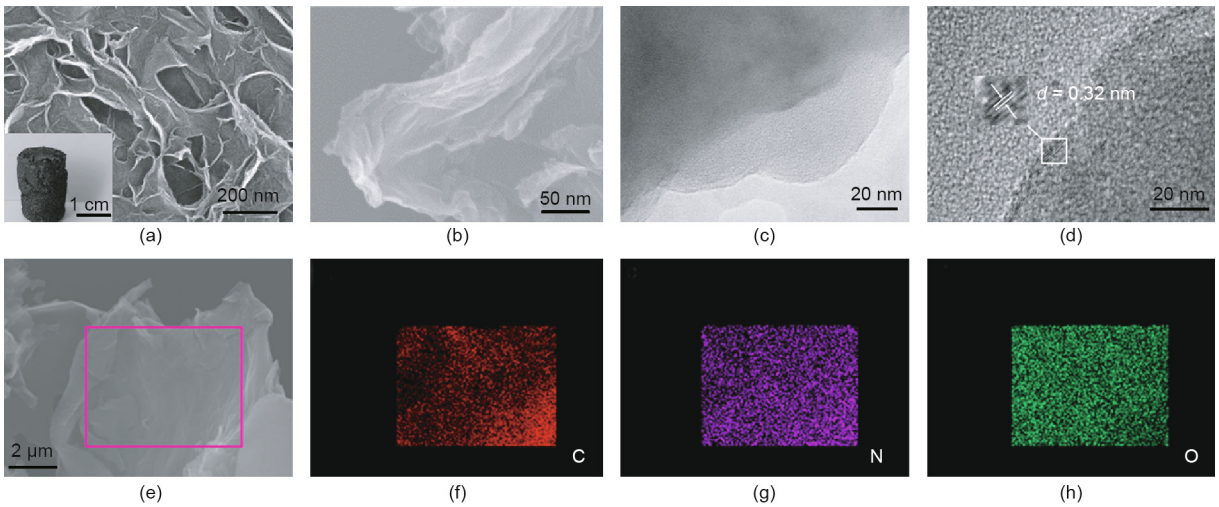


**Fig. 1.** Appearance of the NGF catalyst. (a) The optical microscope image displays the porous structure of the NGF and the inset digital photograph shows a macroscopic regular cylinder-like shape; (b) SEM image of NGF; (c, d) TEM images; (e) SEM image corresponding element mapping images for (f) C, (g) N, and (h) O show a uniform distribution of the elements at mesoscale.

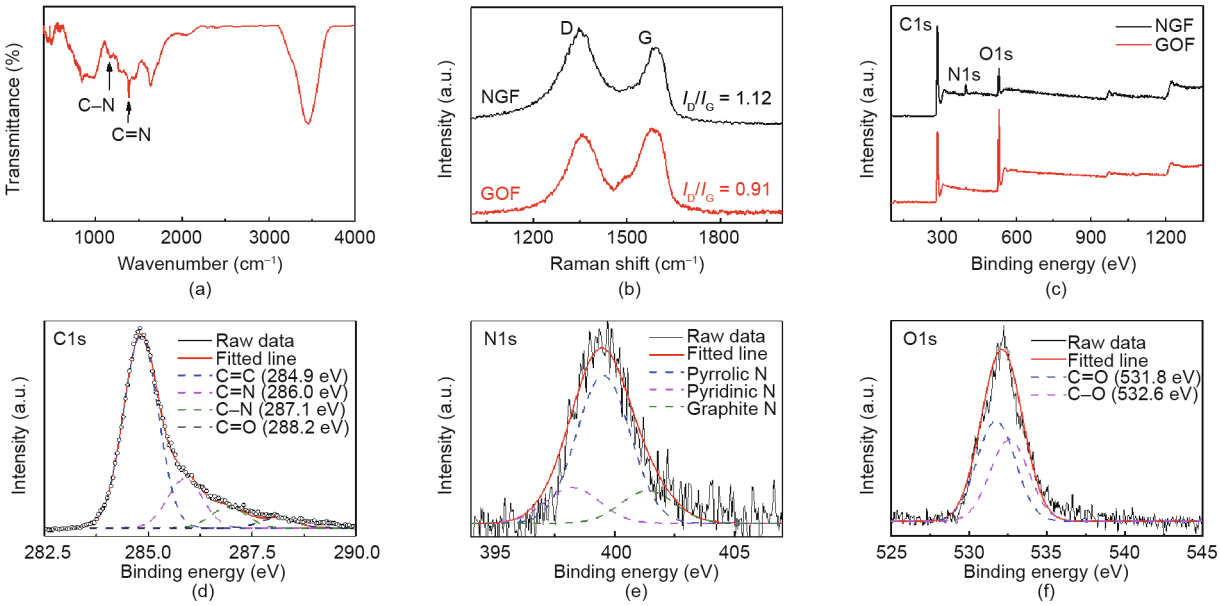


**Fig. 2.** Chemical construction of the NGF catalyst. (a) FTIR spectrum, (b) Raman spectra, and (c) XPS survey of the NGF; (d–f) high-resolution C1s, N1s, and O1s spectra of the NGF. GOF: graphene oxide foam.

doping in the graphene sheet. The thermogravimetric analysis (TGA) curves in Fig. S2 show the weight loss of NGF under thermal air conditions; the weight losses between 200 and 550 °C and 550 and 650 °C were attributed to the pyrolysis of oxygen-containing groups and to the burning of NGF, respectively [29]. To verify the change in defect degree due to nitrogen atom doping, Raman analysis was conduct before and after the doping process. As shown in Fig. 2(b), the most characteristic feature is that a 10 $cm^{-1}$ blue shift exists for the G band of the N-doped graphene, in comparison with the GO films [30]. The D band (Raman shift of 1355 $cm^{-1}$) and G band (Raman shift of 1600 $cm^{-1}$) represent the level of defect and ideality of the graphene sheet, respectively. A higher ratio of D to G band intensities ($I_D/I_G$) for NGF (ratio of 1.12) than for GO (ratio of 0.91) indicates increasing defects of the graphene sheet after the N-doping process [31]. Moreover, apart from the D band and G band, there are two excrescent peaks for NGF at about 1450 and 1265 $cm^{-1}$, which indicate the increment of amorphous carbon due to the doping of heteroatoms (Fig. S3) [32]. The chemical composition analyses of NGF and graphene oxide foam (GOF) were further analyzed by XPS; the results are shown in Fig. 2(c). It is clear that the NGF sample exhibits N1s peaks at about 400 eV with an atomic percentage of 7.23%. Conversely, there are no significant N peaks in the GO sheet sample, which indicates the doping of nitrogen atoms in the graphene structure. The carbon atom percentage increased and the oxygen atom percentage decreased for the NGF sample compared with the GO sheet, which was due to the reduction of GO during the nitrogen-doping process. Fig. 2(d) shows that the C1s peak can be decomposed into four peaks at about 284.9, 286.0, 287.1, and 288.2 eV, corresponding to the graphite $sp^2$ C, N-$sp^2$ C, N-$sp^3$ C, and C=O bond, respectively. Fig. 2(e) shows the high-resolution XPS N1s peak of NGF, which can be separated into three components at 398.2, 399.6, and 401.3 eV, corresponding to pyridinic, pyrrolic, and graphitic nitrogen, respectively (Fig. S4). The relative amount is in good

agreement with the results of the theoretical calculation of doping energy (Table S1). The O1s band in Fig. 2(f) includes two peaks at 531.8 and 532.6 eV for C=O and C–O, respectively. The BET specific surface area of the NGF was measured to be 189 $m^2 \cdot g^{-1}$ (Fig. S5(a)). The type-IV isotherm curve with an obvious hysteresis confirms the presence of mesopores. The rapid $N_2$ uptake ($P/P_0 > 0.9$) is attributable to the existence of much larger pores in the NGF. Barrett–Joyner–Halenda (BJH) pore-size distributions examined by $N_2$ desorption confirm that the main mesopores have diameters between 2 and 40 nm [33].

The chemical properties of NGF were simulated by density functional theory (DFT) theoretical calculation. As shown in Fig. S6, the charge density was uniformly distributed on the graphene from the charge density difference and charge density isopycnal. However, the distribution of the charge density was disturbed (Figs. S6(c)–(h)) when nitrogen atoms were doped into the graphene molecule structure. Three kinds of N atoms (graphite N, pyridinic N, and pyrrolic N) were simulated according to the XPS data. The highest occupied molecular orbital (HOMO) and lowest unoccupied molecular orbital (LUMO) of different models are shown in Fig. S7. The main change between the intrinsic graphene and the doped graphene is that the LUMO number increased due to the introduction of nitrogen, which results in better electron-accepting ability of the nitrogen-doped graphene. In addition, the doping energy ($E_{doping}$) of graphite N, pyridinic N, and pyrrolic N were calculated and are listed in Table S1. The results show that the pyrrolic N needs the lowest doping energy, which indicates the greatest possibility for pyrrolic N to be introduced into the graphene molecule in comparison with the other two kinds of N atoms.

To explore the ability of NGF as a catalyst for liquid-phase hydrogenation under various conditions, the reduction of NB to aniline (AB) by $NaBH_4$ was chosen as a model reaction. Fig. 3(a) shows the UV/Vis spectra during the NB reduction process with the NGF; it is apparent that a characteristic absorbance peak of AB at around 232 nm rises as the characteristic absorbance peak of NB at around 267 nm decreases, indicating that the NB is gradually reduced to AB, when compared with the UV/Vis spectrogram of the origin NB and AB (Fig. S8). After 32 min, the adsorption peak of the NB verge stabilizes, indicating that the reaction proceeded to completion. It is noted that an isosbestic point at about 243 nm indicates the only conversion process without producing any byproducts [34]. HPLC analysis also showed that 99% of the NB was converted to AB when the reaction process was completed (Table S2). However, as shown in Fig. S9, in the absence of the catalyst, the NB typical absorption peak at 267 nm is slightly decreased and no AB absorption peak can be observed for a long time (2 h). This indicates that the reduction reaction barely proceeds without the catalyst, with the slight decrease of NB being accredited to its volatilization in air. However, a rapid decrease occurs in the concentration of NB, although no AB peak arises, as the GOF is added into the reactant solution; this is attributed to the strong adsorption of NB by graphene oxide (Fig. S9).

As the concentration of the reductant $NaBH_4$ is fairly excessive for the reactants in the reaction solution ($C_{NB}$:$C_{NaBH_4}$ = 1:100), the reactions obey pseudo-first-order kinetics throughout this study. The value of the apparent kinetic rate constant ($k_{app}$) for this reaction can be calculated by the following equation [35]:

$$\ln\left(\frac{A_t}{A_0}\right) = \ln\left(\frac{C}{C_0}\right) = -k_{app} \cdot t \quad (1)$$

where $A_t$ and $A_0$ are the absorption peaks of NB at any time $t$ and at 0 min, respectively, and $C$ and $C_0$ are the concentration of NB in the solution corresponding to $A_t$ and $A_0$, respectively. The $k_{app}$ (value of 0.0314 $min^{-1}$) of the reduction of NB under room temperature and pressure conditions can be calculated from the slope of the curve-fitting line by the plot of $\ln(C/C_0)$ versus reaction time (Fig. 3(b)). Furthermore, the specific rate constant of NGF under these conditions was calculated as $8.49 \times 10^{-6}$ $mol \cdot (L \cdot s \cdot g)^{-1}$, which is comparable with the work ($8.33 \times 10^{-6}$ $mol \cdot (L \cdot s \cdot g)^{-1}$) of Hu et al. [36].

Fig. 4(a) shows the process for the metal-free reaction system under high gravity. Typically, 6 mg 3D NGF was packed in a tube reactor; 7 mL reactant mixture was then added, containing 2 mmol $NaBH_4$ and 0.02 mmol NB. Different high gravity fields were produced by high-speed centrifuge at varied rotational speeds. Fig. 4(b) displays the values of $\ln(C/C_0)$ versus reaction time at different high gravity levels ($G$); the different reaction rates under different high gravity conditions are shown in Fig. 4(c). It can be seen that the $k_{app}$ of NB increases as the value of $G$ rises, and the maximal value of $k_{app}$ is about six times higher ($k_{app}$ = 0.1545 $min^{-1}$) at a high gravity level of 6484$g$ ($g$ = 9.81 $m \cdot s^{-2}$) than in a conventional reactor. The reaction was also conducted under a high gravity field of 6484$g$ without using NGF catalyst. As shown in Fig. S10, the result is similar to that of the reaction system without a catalyst under normal gravity; that is, the reduction reaction can barely proceed without the catalyst even under a high gravity field. Fig. S11 and Fig. 4(d) show the velocity vector distribution and filament line of the reactant mixture simulated by computational fluid dynamics (CFD), respectively. The flow condition of the liquid decomposes into a radial direction rate and a tangential rate relative to the rotation of the plane for the reaction space, and the radial direction rate can be seen to increase as the value of $G$ rises by comparing the size of the vector velocity line (Fig. S11), which

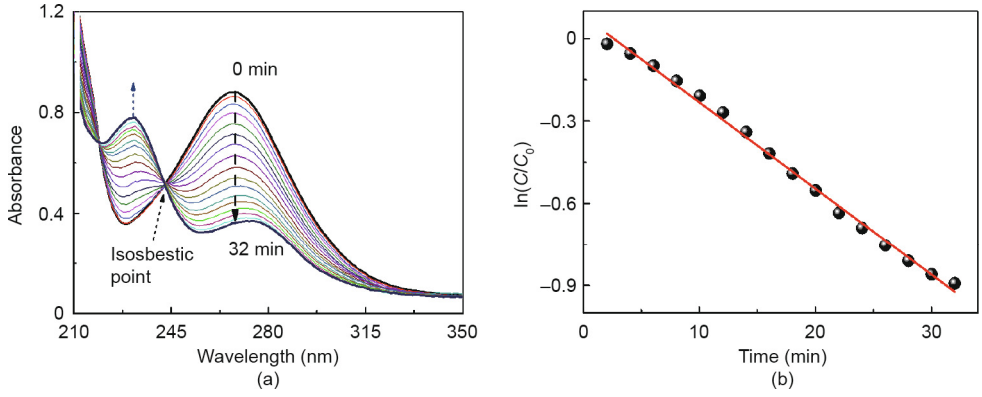


**Fig. 3.** The catalytic performance evaluation for NGF. (a) UV/Vis spectra of the reaction solution; (b) curves of $\ln(C/C_0)$ as a function of time. Reaction conditions: The reaction was carried out at room temperature with 6 mg NGF catalyst presence and 7 mL reactant mixture with an original ratio of $C_{NB}$:$C_{NaBH_4}$, =1:100, and was measured by UV/Vis every 2 min.

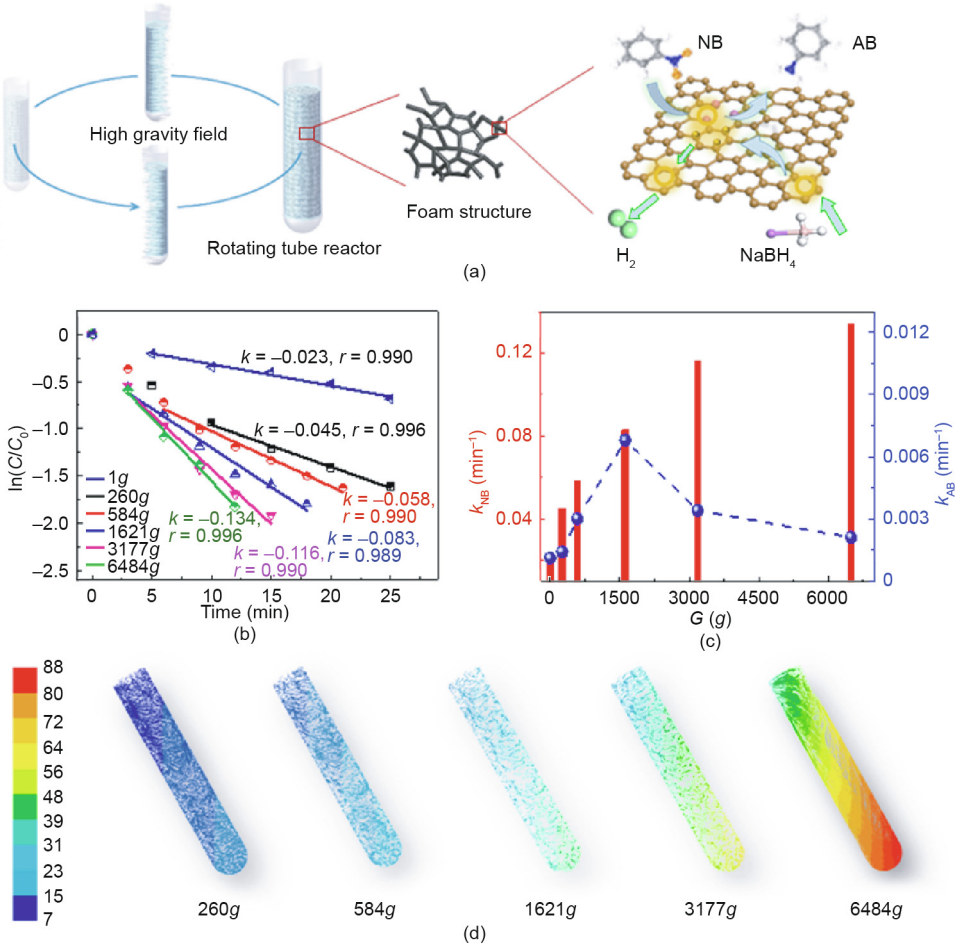


**Fig. 4.** The reduction of nitrobenzene by NGF under a high gravity field. (a) Schematic diagram of the reaction under a high gravity field; (b) $\ln(C/C_0)$ at a wavelength of 267 nm versus reaction time at different high gravity levels ($G$); (c) degradation rate of NB and generation rate of AB versus different $G$; (d) filament line of the reactant mixture simulated by CFD at different high gravity levels (the legend on the left represents the rate ($m \cdot s^{-1}$) of the mixture in the rotating tube reactor).

results in strong turbulence of the mixture in the rotating tube reactor. Due to the strong centrifugal force that is provided by the rotating process, the reactant liquid disintegrates and collides with the bulk porous NGF catalyst in both the radial direction and the tangential direction. This process can greatly increase the chance of contact between the reactant molecules and catalyst, which results in intensification of the adsorption and reaction of the catalytic reduction system.

However, the production rate of AB ($k_{AB}$) increased with the value of $G$ from 1$g$ to 1621$g$, and then decreased with further increasing $G$. The reduction of aromatics normally follows the Langmuir–Hinshelwood mechanism, according to previous studies [37,38]. Taking this into consideration, we suppose that the catalytic reduction of the aromatic initiates the prior adsorption of $NaBH_4$, and then NB is absorbed on the surface of the solid catalyst. The surface-active hydrogen species, which is formed by the decomposition of $NaBH_4$, then reacts with the subsequently adsorbed NB on the surface of the NGF to generate the target products. In the meantime, the surface-active hydrogen species also decomposes into hydrogen and water, and finally leaves the reaction system. Taking all of this into consideration, there are two possible reasons for the decreasing generation rate of the target products: the decomposition of $NaBH_4$ and the competitive adsorption between NB and $NaBH_4$. However, as shown in Fig. 4, the concentration of NB decreased as the absorption and catalytic reaction intensified when the high gravity level ($G$) rose. Therefore, the decomposition of $NaBH_4$ is the main reason for the decreasing generation rate of AB. When the reactants were under a relatively low level of high gravity (i.e., lower than 1621$g$), the formation of the active hydrogen species was rapid and the decomposition rate of $NaBH_4$ over NB was milder, which ensured enough reactive hydrogen species for NB and sufficient time for the surface reaction to occur before the $NaBH_4$ decomposed. When the high gravity level was increased further (up to 6486$g$), the decomposition rate of $NaBH_4$ over NB was much faster, and there was not enough time for the active hydrogen to reduce NB into AB, resulting in a low generation rate of the target product.

The chemical construction of the NGF after the reaction was examined by XPS and Raman spectra; as shown in Fig. 5, there are no obvious differences between the original NGF and the catalyst after the reaction, indicating that the 3D bulk nanocarbon catalyst was stable during the catalytic reaction process. The excellent physical-structure stability of NGF shows its potential for applications of monolithic packing in rotating packing bed (RPB) reactors, a high-gravity equipment mentioned above, which have an intensification mechanism similar to the high gravity field study in this work. Our group has studied mass-transfer processes and scale-up laws for many years. Wang et al. [10] conducted the catalytic oxidation of benzylic alcohols in an RPB reactor, and the results showed that the conversion of benzylic alcohols increased from 5.56% (in conventional STR) to 20.86% (in RPB) even in a scale-up level. Up to now, the RPB has been applied to industrial production, but the gravity level is still limited (less than 1000$g$); the present work provides a new method to achieve a higher gravity level

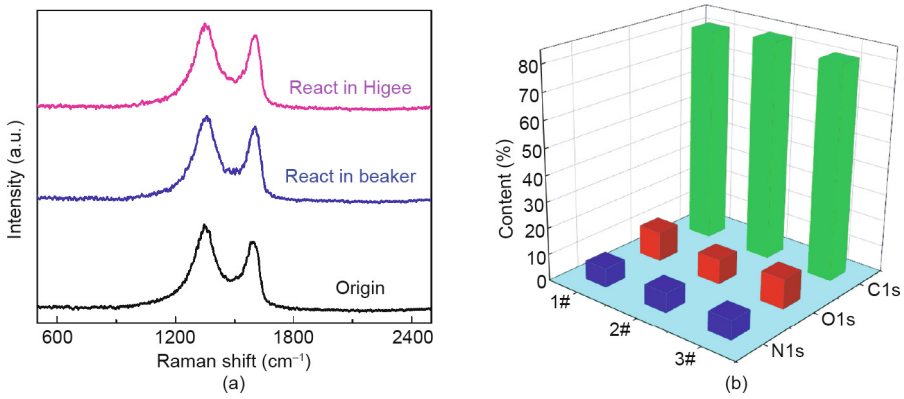


**Fig. 5.** Stability performance of NGF. (a) Raman spectra; (b) element ratio of NGF measured by XPS before and after the reaction (where "#1," "#2," and "#3" represent the NGF catalyst of the original, after reacting under a normal gravity field, and after reacting under a high gravity (Higee) field, respectively).

and shows great potential for ultra-high gravity intensification applications in metal-free catalytic reactions.

Furthermore, the catalytic degradation of MB, an important reaction for environmental protection, was also operated in a high-gravity environment to verify the trend of intensification. The UV–Vis spectra of the MB reduction process are shown in Fig. S12, and the decreasing trend of the absorption intensity at about 665 nm indicates the reduction of MB. In the kinetics study, the relative absorbance of the band at 665 nm was plotted as a function of time to evaluate the reduction reaction rate. In order to exclude the influence of sunlight, we first carried out the degradation reaction of MB under five different conditions: pure MB stewing under sunlight, MB stewing under sunlight with $NaBH_4$, MB stewing under sunlight with $NaBH_4$ and NGF, MB stewing in the dark with $NaBH_4$, and MB stewing in the dark with $NaBH_4$ and NGF (Fig. S13). The results indicate that sunlight has almost no effect on the process of MB degradation, and the reaction barely proceeded without the NGF catalyst. Taking both the degree of fitting and the reaction mechanism into consideration, first-order kinetics is the most suitable. Thus, in subsequent work, the error result from the sunlight was ignored and first-order kinetics was chosen for further analysis. Regarding the influence of the high gravity field, Fig. 6(a) shows the $\ln(C/C_0)$ of the reaction mixture after reacting for 1 h under six different reaction conditions. When there is no NGF catalyst in the reaction mixture, the MB will not degrade, regardless of whether or not $NaBH_4$ is added, under the high gravity conditions. Comparing the reaction rate of Sample #3 (or Sample #4) with that of Sample #5 (or Sample #6) in Fig. 6(b) reveals that the degradation rates of MB show a sharp increase when the reaction occurs under high-gravity conditions. Fig. 7 shows the rate of MB degradation increasing as the high gravity level gradually increases, which agrees with the results of the NB catalytic reduction system. In particular, a slight difference in the increasing rate of the reaction along the *G* between two reaction systems is due to the different ability of adsorption for reactants on the NGF catalyst. For the NB system, the reductant was adsorbed onto the active site prior to the adsorption of NB molecules; thus, the $NaBH_4$ was adequate for the reaction to proceed, resulting in a sharp rate increase under a lower level of high gravity field. However, for the reduction of MB, the reactant molecules may be protonated to form protonated and cationic species in order to form reduced and protonated leuco-MB. As soon as $NaBH_4$ provides electrons to the catalyst, the generated radicals react with the functional group of the adsorbed MB; this means that the MB molecules and the $NaBH_4$ reductant are adsorbed simultaneously onto the surface of NGF, resulting in a lower increase in the rate in a lower gravity field but a rapid increase in the rate in a high gravity field [39].

## 4. Conclusions

3D bulk NGF was prepared by a hydrothermal method and exhibited high performance as a catalyst for NB reduction and MB degradation. Compared with traditional powder catalysts, 3D bulk catalysts are more convenient to separate from the products and more promising for industrial applications. The metal-free catalyst was then used as packing under high-gravity conditions in a rotating tube reactor. The apparent rate constant ($k_{app}$) of the reduced reaction in the rotating tube reactor (high gravity level of 6484*g*) was more than six times greater than that in a conventional reactor. The excellent catalytic efficiency of the NGF catalyst

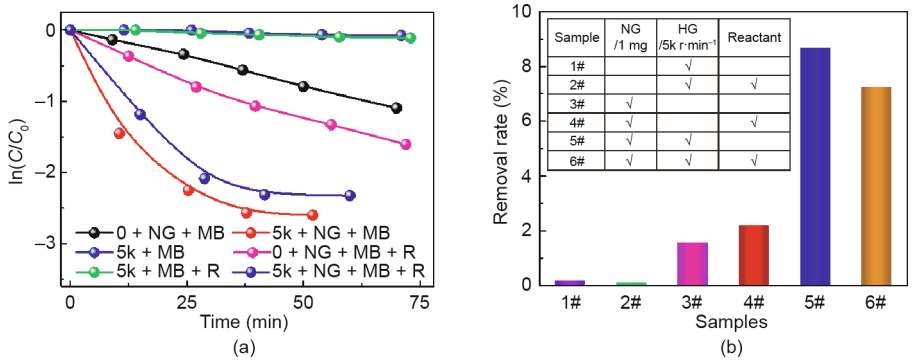


**Fig. 6.** Degradation reaction of MB under different conditions. (a) $\ln(C/C_0)$ versus time; (b) degradation rate under different reaction conditions (where "5k" represents the rotating speed of 5000 r·min$^{-1}$ and "R" represents the existence of the reductant).

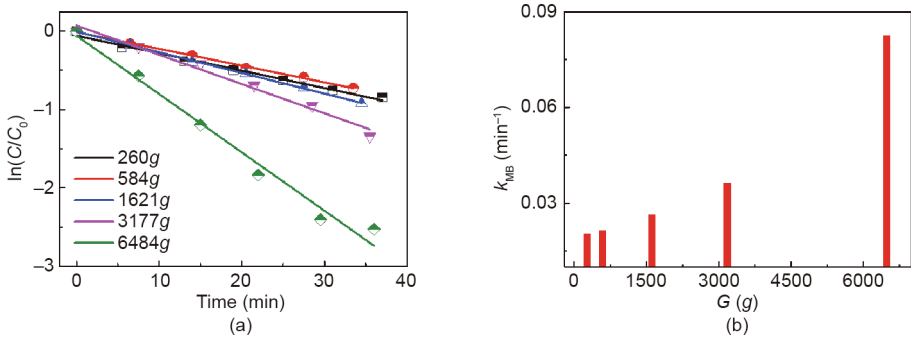


**Fig. 7.** Reduction of MB by NGF catalyst under a high gravity field. (a) $\ln(C/C_0)$ at a wavelength of 664 nm versus reaction time at different $G$; (b) degradation rate of MB versus different $G$.

under a high gravity field demonstrates the potential to use high-gravity technology for the intensification of metal-free catalytic reactions.

## Acknowledgements

We are grateful for financial support from National Natural Science Foundation of China (21620102007) and the Fundamental Research Funds for the Central Universities of China (JD2002).

## Compliance with ethics guidelines

Zhiyong Wang, Zhijian Zhao, Jesse Baucom, Dan Wang, Liming Dai, and Jian-Feng Chen declare that they have no conflict of interest or financial conflicts to disclose.

## Appendix A. Supplementary data

Supplementary data to this article can be found online at https://doi.org/10.1016/j.eng.2019.12.018.

## References

[1] Gong K, Du F, Xia Z, Durstock M, Dai L. Nitrogen-doped carbon nanotube arrays with high electrocatalytic activity for oxygen reduction. Science 2009;323(5915):760–4.
[2] Geim AK, Grigorieva IV. Van der Waals heterostructures. Nature 2013;499(7459):419–25.
[3] Hu CG, Lin Y, Connell JW, Cheng HM, Gogotsi Y, Titirici M, et al. Carbon-based metal-free catalysts for energy storage and environmental remediation. Adv Mater 2019;31(13):1806128.
[4] Dai L. Metal-free carbon electrocatalysts: recent advances and challenges ahead. Adv Mater 2019;31(13):1900973.
[5] Wang Z, Pu Y, Wang D, Wang JX, Chen JF. Recent advances on metal-free graphene-based catalysts for the production of industrial chemicals. Front Chem Sci Eng 2018;12(4):855–66.
[6] Wang D, Chen KQ, Cheng DG, Peng C, Zhang JT. Green catalytic engineering: a powerful tool for sustainable development in chemical industry. Front Chem Sci Eng 2018;12(4):835–7.
[7] Zhang J, Liu X, Blume R, Zhang A, Schlögl R, Su DS. Surface-modified carbon nanotubes catalyze oxidative dehydrogenation of *n*-butane. Science 2008;322(5898):73–7.
[8] Li X, Pan X, Yu L, Ren P, Wu X, Sun L, et al. Silicon carbide-derived carbon nanocomposite as a substitute for mercury in the catalytic hydrochlorination of acetylene. Nat Commun 2014;5:3688–94.
[9] Tang P, Hu G, Li M, Ma D. Graphene-based metal-free catalysts for catalytic reactions in the liquid phase. ACS Catal 2016;6(10):6948–58.
[10] Wang Z, Shi J, Wang D, Pu Y, Wang JX, Chen JF. Metal-free catalytic oxidation of benzylic alcohols for benzaldehyde. React Chem Eng 2019;4(3):507–15.
[11] Wang B. The future of manufacturing: a new perspective. Engineering 2018;4(5):722–8.
[12] Yin S, Chen K, Srinivasakannan C, Guo S, Li S, Peng J, et al. Enhancing recovery of ammonia from rare earth wastewater by air stripping combination of microwave heating and high gravity technology. Chem Eng J 2018;337:515–21.
[13] Liu Y, Bai J, Duan H, Yin X. Static magnetic field-assisted synthesis of $Fe_3O_4$ nanoparticles and their adsorption of Mn(II) in aqueous solution. Chin J Chem Eng 2017;25(1):32–6.
[14] Yu Y, Bai S, Wang S, Hu A. Ultra-short pulsed laser manufacturing and surface processing of microdevices. Engineering 2018;4(6):779–86.
[15] Tian Y, Demirel SE, Hasan MMF, Pistikopoulos EN. An overview of process systems engineering approaches for process intensification: state of the art. Chem Eng Process 2018;133:160–210.
[16] Leng J, Chen J, Wang D, Wang JX, Pu Y, Chen JF. Scalable preparation of $Gd_2O_3$:$Yb^{3+}$/$Er^{3+}$ upconversion nanophosphors in a high-gravity rotating packed bed reactor for transparent upconversion luminescent films. Ind Eng Chem Res 2017;56(28):7977–83.
[17] Pu Y, Leng J, Wang D, Wang JX, Foster NR, Chen JF. Process intensification for scalable synthesis of ytterbium and erbium co-doped sodium yttrium fluoride upconversion nanodispersions. Powder Technol 2018;340:208–16.
[18] He X, Tang R, Pu Y, Wang JX, Wang Z, Wang D, et al. High-gravity-hydrolysis approach to transparent nanozirconia/silicone encapsulation materials of light emitting diodes devices for healthy lighting. Nano Energy 2019;62:1–10.
[19] Guo J, Jiao W, Qi G, Yuan Z, Liu Y. Applications of high-gravity technologies in gas purifications: a review. Chin J Chem Eng 2019;27(6):1361–73.
[20] Qin Y, Luo S, Geng S, Jiao W, Liu Y. Degradation and mineralization of aniline by $O_3$/Fenton process enhanced using high-gravity technology. Chin J Chem Eng 2018;26(7):1444–50.
[21] Luo Y, Luo JZ, Chu GW, Zhao ZQ, Arowo M, Chen JF. Investigation of effective interfacial area in a rotating packed bed with structured stainless steel wire mesh packing. Chem Eng Sci 2017;170:347–54.
[22] Guo Q, Liu Y, Qi G, Jiao W. Study of low temperature combustion performance for composite metal catalysts prepared via rotating packed bed. Energy 2019;179:431–41.
[23] Jiao W, Qiao J, Qin Y, Liu Y. Effects of coexisting substances on aniline degradation with ozone-based advanced oxidation process in high-gravity fields. Chem Eng Process 2019;138:36–40.
[24] Zhang WJ, Zhang B, Shi ZQ. Study on hydrodynamic performance and mass transfer efficiency of nickel foam packing. Procedia Eng 2011;18:271–6.
[25] Lévêquer J, Rouzineau D, Prévost M, Meyer M. Hydrodynamic and mass transfer efficiency of ceramic foam packing applied to distillation. Chem Eng Sci 2017;64(11):2607–16.
[26] Li D, Müller MB, Gilje S, Kaner RB, Wallace GG. Processable aqueous dispersions of graphene nanosheets. Nat Nanotechnol 2008;3(2):101–5.
[27] Guo HL, Su P, Kang XF, Ning SK. Synthesis and characterization of nitrogen-doped graphene hydrogels by hydrothermal route with urea as reducing-doping agents. J Mater Chem A 2013;1(6):2248–55.
[28] Kangvansura P, Chew LM, Kongmark C, Santawaja P, Ruland H, Xia W, et al. Effects of potassium and manganese promoters on nitrogen-doped carbon nanotube-supported iron catalysts for $CO_2$ hydrogenation. Engineering 2017;3(3):385–92.
[29] Liu J, Yan X, Wang L, Kong L, Jian P. Three-dimensional nitrogen-doped graphene foam as metal-free catalyst for the hydrogenation reduction of *p*-nitrophenol. J Colloid Interface Sci 2017;497:102–7.
[30] Lin D, Hu C, Chen H, Qu J, Dai L. Microporous N,P-codoped graphitic nanosheets as an efficient electrocatalyst for oxygen reduction in whole pH range for energy conversion and biosensing dissolved oxygen. Chem Eur J 2018;24(69):18487–93.
[31] Wang Z, Su R, Wang D, Shi J, Wang JX, Pu Y, et al. Sulfurized graphene as efficient metal-free catalysts for reduction of 4-nitrophenol to 4-aminophenol. Ind Eng Chem Res 2017;56(46):13610–7.
[32] Wang Z, Pu Y, Wang D, Shi J, Wang JX, Chen JF. 3D-foam-structured nitrogen-doped graphene-Ni catalyst for highly efficient nitrobenzene reduction. AIChE J 2018;64(4):1330–8.
[33] Hu C, Dai L. Multifunctional carbon-based metal-free electrocatalysts for simultaneous oxygen reduction, oxygen evolution, and hydrogen evolution. Adv Mater 2017;29(9):4942–50.

[34] Kästner C, Thünemann AF. Catalytic reduction of 4-nitrophenol using silver nanoparticles with adjustable activity. Langmuir 2016;32(29):7383–91.
[35] Khan SR, Farooqi ZH, Zaman WU, Ali A, Begum R, Kanwal F, et al. Kinetics and mechanism of reduction of nitrobenzene catalyzed by silver-poly (*n*-isopropylacryl amide-*co*-allylacetic acid) hybrid microgels. Mater Chem Phys 2016;171:318–27.
[36] Hu H, Xin JH, Hu H, Wang X. Structural and mechanistic understanding of an active and durable graphene carbocatalyst for reduction of 4-nitrophenol at room temperature. Nano Res 2015;8(12):3992–4006.
[37] Yang JH, Sun G, Gao Y, Zhao H, Tang P, Tan J, et al. Direct catalytic oxidation of benzene to phenol over metal-free graphene-based catalyst. Energy Environ Sci 2013;6(3):793–8.
[38] Wunder S, Lu Y, Albrecht M, Ballauff M. Catalytic activity of faceted gold nanoparticles studied by a model reaction: evidence for substrate-induced surface restructuring. ACS Catal 2011;1(8):908–16.
[39] Vidhu VK, Philip D. Catalytic degradation of organic dyes using biosynthesized silver nanoparticles. Micron 2014;56:54–62.